Nanoscale

PAPER

View Article Online
View Journal | View Issue

Cite this: *Nanoscale*, 2024, **16**, 3011

A rapid and specific antimicrobial resistance detection of *Escherichia coli via* magnetic nanoclusters†

Fei Pan, *‡[a] Stefanie Altenried,[a] Subas Scheibler[b,c] and Qun Ren *[a]

Received 29th October 2023,
Accepted 11th January 2024

DOI: 10.1039/d3nr05463b

rsc.li/nanoscale

Drinking water contamination, often caused by bacteria, leads to substantial numbers of diarrhea deaths each year, especially in developing regions. Human urine as a source of fertilizer, when handled improperly, can contaminate drinking water. One dominant bacterial pathogen in urine is *Escherichia coli*, which can trigger serious waterborne/foodborne diseases. Considering the prevalence of the multi-drug resistant extended-spectrum beta-lactamase (ESBL) producing *E. coli*, a rapid detection method for resistance is highly desired. In this work, we developed a method for quick identification of *E. coli* and, at the same time, capable of removal of general bacterial pathogens from human urine. A specific peptide GRHIFWRRGGGHKVAPR, reported to have a strong affinity to *E. coli*, was utilized to modify the PEGylated magnetic nanoclusters, resulting in a specific capture and enrichment of *E. coli* from the bacteria-spiked artificial urine. Subsequently, a novel luminescent probe was applied to rapidly identify the antimicrobial resistance of the collected *E. coli* within 30 min. These functionalized magnetic nanoclusters demonstrate a promising prospect to rapidly detect ESBL *E. coli* in urine and contribute to reducing drinking water contamination.

Introduction

Bacterial contamination of drinking water is a leading cause of waterborne diseases in rural areas of most developing regions.[1–4] The existence of antimicrobial-resistant bacteria in contaminated drinking water can cause serious health concerns.[5] Urine is a common source of fertilizer, and its flushing, without careful treatment, can lead to water contamination. The dominant bacterial pathogen in urine is *Escherichia coli*,[6] which can trigger serious waterborne/foodborne diseases.[7,8] Thereby, it is highly desired to know the presence and subsequently remove the antimicrobial-resistant bacteria in urine before its emission.

Substantial efforts have been dedicated to identifying bacterial pathogens and rapidly sensing bacterial resistance,[9–12] *e.g.*, single-cell morphological analysis based on microscopic analysis of cell growth[10] and localized surface plasmon resonance towards the evaluation of bacterial lysis.[13] However, the great challenges for the diagnostics of antimicrobial resistance have not been overcome. The turnaround time is still very long, especially for samples containing the target species at low concentrations. In this regard, the time-consuming pre-culture steps cannot be avoided to enrich the present bacterial pathogens and the subsequent purification. Various strategies to circumvent the pre-culture steps have been tackled. Antibodies have also been used to enrich bacteria due to their high specificity toward target antigens on the surfaces of pathogens.[9–12,14] However, the preparation of antibodies is complex and costly, limiting the availability of antibodies for establishing specific targeting systems and hindering their application.[15] Moreover, due to the large size of antibodies as well as the difficulty of functionalizing antibodies to an anticipated surface (*e.g.*, spherical surfaces), their application potential for particle-based detection of pathogenic bacteria has been limited.[15] Additionally, some antibiotics, proteins (*e.g.*, avidin, biotin, and lectin), DNA/RNA aptamers, and carbohydrates (such as glycan) have displayed their application potential as specific targeting ligands to capture bacteria.[16] However, the limited specificity still remains a challenge to be

[a]*Laboratory for Biointerfaces, Empa, Swiss Federal Laboratories for Materials Science and Technology, Lerchenfeldstrasse 5, 9014 St. Gallen, Switzerland. E-mail: fei.pan@empa.ch, phoenix.pan@tum.de, qun.ren@empa.ch*
[b]*Nanoparticle Systems Engineering Laboratory, Institute of Process Engineering, Department of Mechanical and Process Engineering, ETH Zürich, Sonneggstrasse 3, 8092 Zürich, Switzerland*
[c]*Laboratory for Particles Biology Interactions, Empa, Swiss Federal Laboratories for Materials Science and Technology, Lerchenfeldstrasse 5, 9014 St. Gallen, Switzerland*
†Electronic supplementary information (ESI) available. See DOI: **https://doi.org/10.1039/d3nr05463b**
‡Present address: Department of Chemistry, University of Basel, Mattenstrasse 24a, BPR 1096, Basel, Switzerland. (fei.pan@unibas.ch)

overcome. Therefore, we designed a diagnostic method to handle the aforementioned challenges through precise isolation of *E. coli* without a pre-culture by exploiting a specific peptide.

Magnetic nanoparticles (MNPs) have been developed to isolate and eradicate bacterial pathogens associated with water contaminations and can additionally target specific species after proper surface functionalization.[17] Since *E. coli* is the predominant bacterial pathogen associated with urine,[18] it is highly desired to design MNPs to specifically capture *E. coli* for subsequent identification of its presence and antimicrobial resistance. A peptide library has been utilized to screen peptides that can specifically bind to *E. coli*,[19] and one specific peptide, namely GRHIFWRRGGGHKVAPR, was identified. In our work here, we exploited this peptide to functionalize magnetic particles, attempting a specific capture and enrichment of *E. coli* to achieve a fast detection of *E. coli* (Scheme 1). The functionalized PEGylated MNCs (peptide@PEG@MNCs) with GRHIFWRRGGGHKVAPR not only enabled a quick non-specific isolation of various bacteria from infected media but also led to a specific capture of *E. coli* even at a concentration as low as 10^0 CFU mL^{-1}. The high specificity between the tested *E. coli* and peptide@PEG@MNCs was, in addition, investigated and confirmed through direct quantitative measurement using a FluidFM. The antimicrobial susceptibility of the captured *E. coli* was moreover analyzed by applying a sensitive luminescent probe, which allowed differentiation of the captured resistant and susceptible *E. coli* within 30 min, faster than the so far reported methods.[10] Therefore, the developed peptide@PEG@MNCs manifest their promising potential in the rapid detection of antimicrobial resistant *E. coli* and reducing *E. coli* infections.

Results and discussion

GRHIFWRRGGGHKVAPR peptide, which binds *E. coli* specifically,[19] was conjugated to the commercial PEGylated magnetic nanoclusters (PEG@MNCs) by the covalent bonding between -COOH and $-NH_2$ (Scheme 1a). Different peptide concentrations were employed for the modification, and the functionalized PEG@MNCs were analyzed for their surface chemistry by X-ray photoelectron spectroscopy (XPS). The measured [C]/[O] elemental ratios were 76.0 ± 0.5%, 98.3 ± 0.6%, 136.7 ± 2.6%, 323.7 ± 2.8%, and 196.1 ± 2.9%, respectively, for the peptide concentrations of 0.02, 0.2, 1, 2 and 20 mM (Fig. 1a). The modification by peptide solution of 2 mM led to the highest [C]/[O] elemental ratio, probably due to the conjugation saturation of the peptide with PEG@MNCs at higher peptide concentration; thus, 2 mM was used in the following studies.

The peptide@PEG@MNCs displayed a size of 155.9 ± 1.4 nm in diameter, larger than the non-modified PEG@MNCs (143.4 ± 1.3 nm in diameter) (Fig. 1b and Fig. S1 a, b†), based on the dynamic light scattering measurement. Additionally, the functionalization retained the magnetic property of the nanoclusters (Fig. S1c†) and did not show cytotoxicity based on the MTS analysis (Fig. S1d†). The capture capacity of peptide@PEG@MNCs was further investigated towards bacteria of different concentrations, employing susceptible *E. coli* as a model strain. The peptide@PEG@MNCs manifested a capability to capture *E. coli* even in an extremely low concentration range of 10^0 CFU mL^{-1}. However, the capture efficiency decreased once the bacterial concentration rose above 10^6 CFU mL^{-1} (Fig. 1c), probably due to the saturation of bacterial capture by a given amount of peptide@PEG@MNCs. Hence, we employed a bacterial suspension of a concentration below 10^6 CFU mL^{-1} for subsequent analysis. Thereupon, bacterial concentrations of 10^5 CFU mL^{-1} were applied to assess the specificity of the peptide@PEG@MNCs towards susceptible and resistant *E. coli*, *Pseudomonas aeruginosa*, *Staphylococcus aureus*, and *Staphylococcus epidermidis* (Fig. 1d). Over 80% of capture efficiency was achieved towards all evaluated bacteria in 10 minutes, demonstrating that the developed peptide@PEG@MNCs could efficiently isolate bacterial pathogens from an infected medium (Fig. 1d). The captured *E. coli* was afterwards analyzed for antimicrobial resistance by employing an AquaSpark luminescent dye (Fig. 1e and Fig. S1e†) and measurement of optical density (OD, Fig. 1f and Fig. S1f†). The luminescent assay allowed a clear differentiation in the growth profile of the susceptible and resistant *E. coli* after an incubation of 30 min in the presence of the antibiotic ampicillin, whereas no clear difference could be noticed through the conventional OD analysis. Without the need for pre-enrichment, this luminescent assay confers eight times faster detection than the previously reported four hours using microscope analysis.[10] In addition, OD is an optical method, which was measured at 600 nm in our investigation of bacterial culture. The reliable OD measured by a lab device is often in a range of 0.05–1, which usually corresponds to a bacterial concentration of 10^6–10^8 CFU mL^{-1}. Such aforementioned concentration (detection limit) is too high to differentiate a growth below 10^6 CFU mL^{-1}, thus making the fast discrimination of resistant and susceptible strains impossible.

Since unspecific interaction can occur between bacteria and nanocluster,[20] we introduced a rinsing process to minimize and avoid the intervention of non-specific binding. *S. aureus* and susceptible *E. coli* were utilized as example strains. It was found that after each time rinsing, the capture efficiency reduced (Fig. 2a). A five-time rinsing process yielded the disappearance of *S. aureus* from the collected peptide@PEG@MNCs, but still about 49% of capture efficiency for *E. coli* (Fig. 2a). Therefore, the rinsing process removed the non-specific weakly attached bacteria from peptide@PEG@MNCs, while the strongly bound bacteria retained, yielding a specific capture. The binding of the susceptible *E. coli* to peptide@PEG@MNCs after the rinsing process can also be observed through TEM analysis (Fig. S1g–i†) after applying diluted peptide@PEG@MNCs samples (100-fold dilution), which can lead to a clear observation of such binding interaction. Hence, the designed peptide@PEG@MNCs led to, on the one hand, the quick isolation of bacterial pathogens

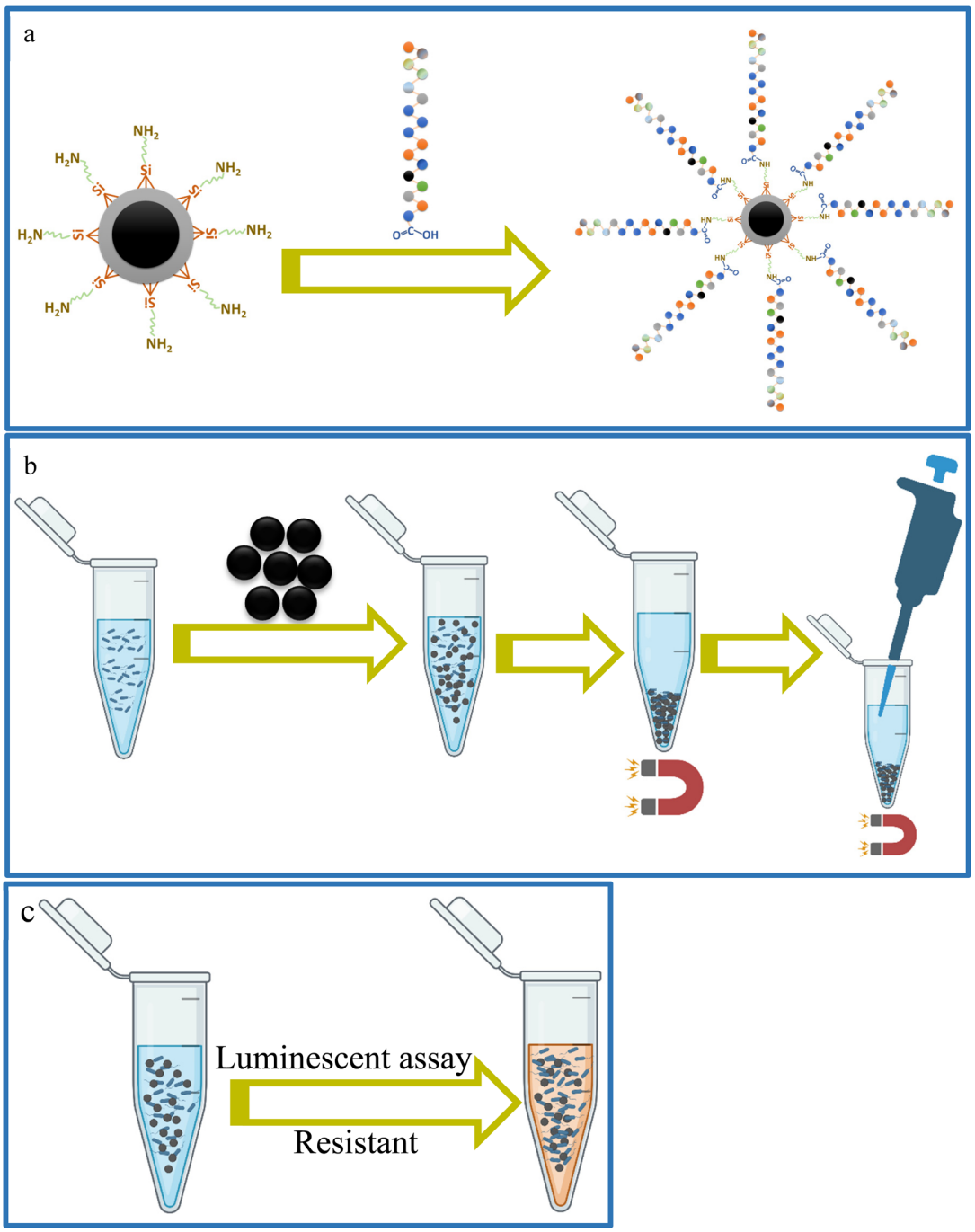

Scheme 1 Schematical illustration of the AMR sensing toward *E. coli*. (a) GRHIFWRRGGGHKVAPR peptide was conjugated to the PEGylated magnetic nanoclusters (PEG@MNCs) by the covalent bonding between –COOH and $-NH_2$. (b) The peptide-functionalized magnetic nanoclusters (peptide@PEG@MNCs) interacted with the bacterial suspensions, and the bacteria attached to the peptide@PEG@MNCs were thereafter collected under a magnetic field. The collected bacteria can be further analyzed with and without a rinsing step. (c) AMR analysis was conducted using a sensitive luminescent assay, where the growth of the collected bacteria can be investigated in the presence of antibiotics to differentiate the susceptible and resistant bacterial pathogens.

without the rinsing process and, on the other hand, a specific capture of *E. coli* after the rinsing process.

The capture specificity of peptide@PEG@MNCs with the rinsing process was further analyzed towards *E. coli* (both susceptible and resistant strains), *P. aeruginosa*, *S. aureus*, and *S. epidermidis* employing MNCs, PEG@MNCs, and peptide@MNCs as controls (Fig. 2). Only *E. coli* (susceptible and resistant strains) were captured after incubating with peptide@PEG@MNCs, while the other tested strains and nanoclusters did not lead to a detectable capture (Fig. 2b).

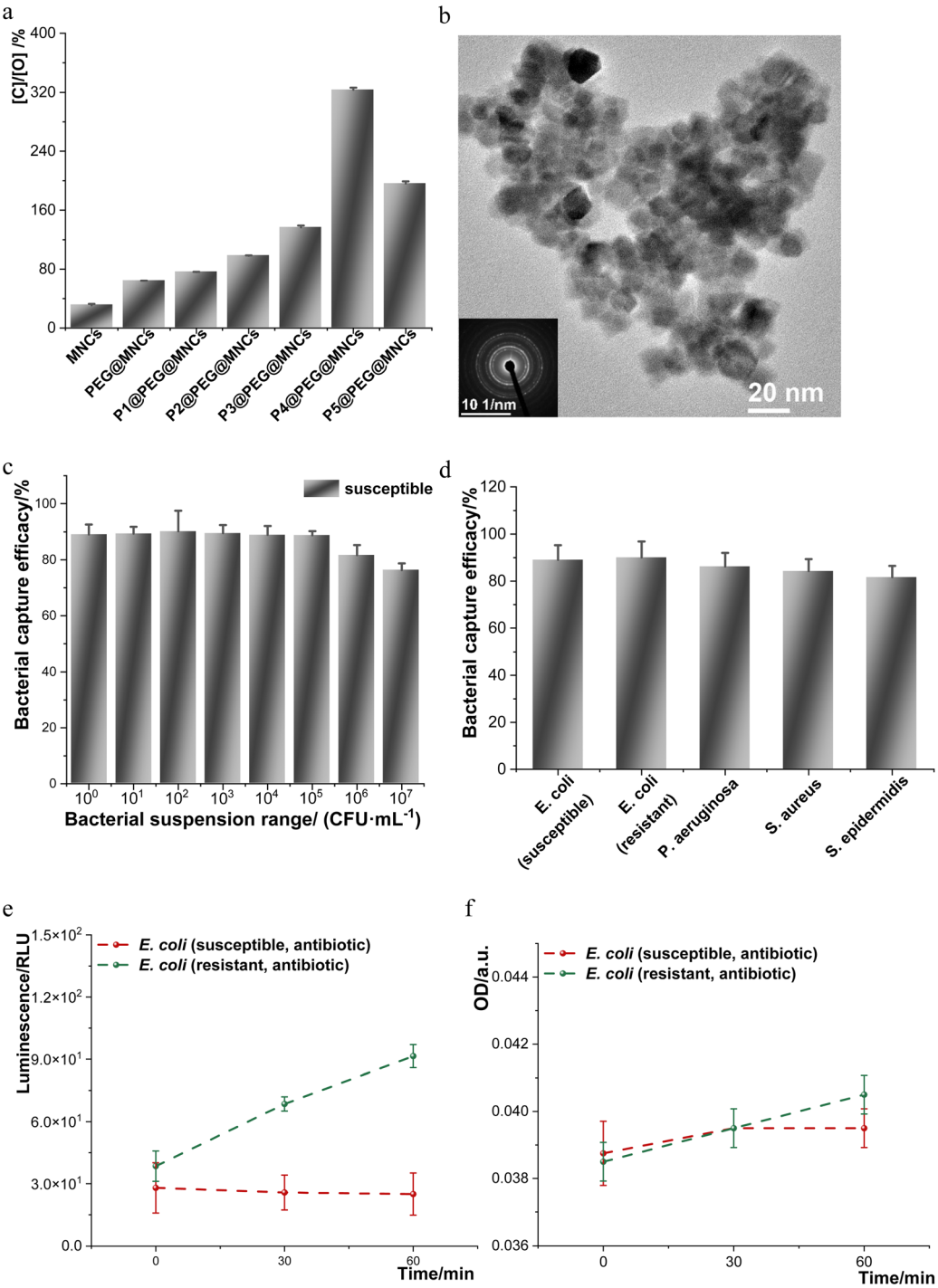

Fig. 1 Characterization of the modified MNCs and the capture capability towards different bacterial strains without the rinsing process. (a) [C]/[O] elemental ratio was measured by employing XPS to assess the modification efficiency of the PEGylated MNCs by the peptide solutions of various concentrations. P1–P5 denote peptide solutions of 0.02, 0.2, 1, 2, and 20 mM, respectively. (b) PEGylated MNCs functionalized with peptide solution of 2 mM (peptide@PEG@MNCs) were imaged by applying a scanning transmission electron microscope (STEM), displaying a cluster structure, which was further confirmed by the respective electron diffraction in the inset. (c) Bacterial capture capability of the modified MNCs was analyzed towards susceptible *E. coli* of different ranges of concentration and normalized to the concentration of the initial bacterial suspension at each range (an initial bacterial suspension of 81 900 000 ± 2 800 000 CFU mL^{-1} was regarded for the range of 10^7 CFU mL^{-1}, and the rest from 10^6–10^0 CFU mL^{-1} was stepwise 10 fold diluted till a concentration range of 10^0 CFU mL^{-1} from the bacterial suspension in a concentration range of 10^7 CFU mL^{-1}). (d) The bacterial capture efficiencies by peptide@PEG@MNCs without a rinsing process towards susceptible and resistant *E. coli*, *P. aeruginosa*, *S. aureus*, and *S. epidermidis*, were respectively normalized to the initial concentration of 156 000 ± 17 000, 302 000 ± 8000, 520 000 ± 27 000, 738 000 ± 21 000 and 531 000 ± 61 000 CFU mL^{-1}. The bacterial growth of the captured susceptible and resistant *E. coli* without a rinsing process was analyzed in the presence of 300 μg mL^{-1} ampicillin through AquaSpark® beta-D-glucuronide (e) and optical density (f). n = 3 (biological repeats), mean ± SD shown; at least two sets of independent experiments were performed, and one set of data is shown.

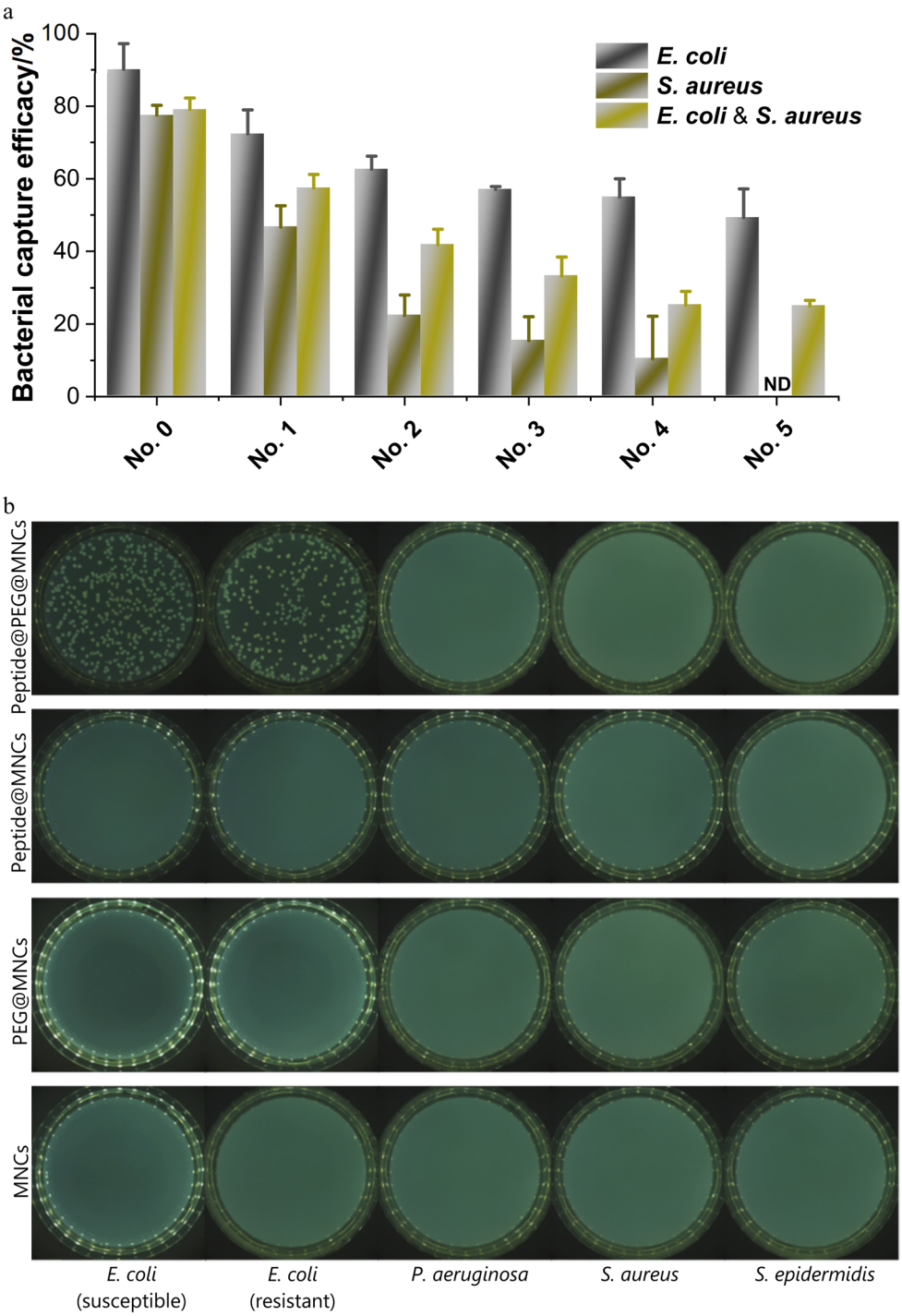

Fig. 2 Specific bacterial capture in PBS towards *E. coli* with a rinsing process. (a) The bacterial capture efficiencies were analyzed through the modified MNCs by a sequential rinsing process up to 5 times to yield a specific capture of *E. coli* towards susceptible *E. coli*, *S. aureus*, and a mixture of susceptible *E. coli* and *S. aureus*. Initial concentrations of *E. coli* and *S. aureus* were respectively 192 000 ± 7000 and 234 000 ± 15 000 CFU mL^{-1}. (b) Specific bacterial capture analysis through MNCs, PEG@MNCs, peptide@MNCs, and peptide@PEG@MNCs towards susceptible and resistant *E. coli*, *P. aeruginosa*, *S. aureus*, and *S. epidermidis*. n = 3 (biological repeats). (c) Affinity assessment between different bacteria and modified/non-modified MNCs by employing single bacterial force spectroscopy. According to the reported methods, modified/non-modified MNCs were deposited on glass Petri dishes coated with polydopamine as an adhesive layer according to the reported methods.[59] (d) Bacterial capture rate through peptide@PEG@MNCs was analyzed for 5, 10, 30, 60, 90, and 120 min interaction towards susceptible and resistant *E. coli*. Each initial bacterial suspension concentration is 673 000 ± 140 000 and 573 000 ± 9000 CFU mL^{-1} for susceptible and resistant *E. coli*. (e) Bacterial capture sensitivity by modified PEG@MNCs was evaluated towards susceptible and resistant *E. coli* of concentrations at various ranges of 10^5–10^0 CFU mL^{-1}, which were stepwise one order of magnitude lower than the bacterial suspension in the range of 10^5 CFU mL^{-1}. Each initial bacterial suspension concentration is 755 000 ± 31 000 and 624 000 ± 73 000 CFU mL^{-1} for susceptible and resistant *E. coli*. n = 3 (biological repeats), mean ± SD shown, for (a), and (d) & (e).

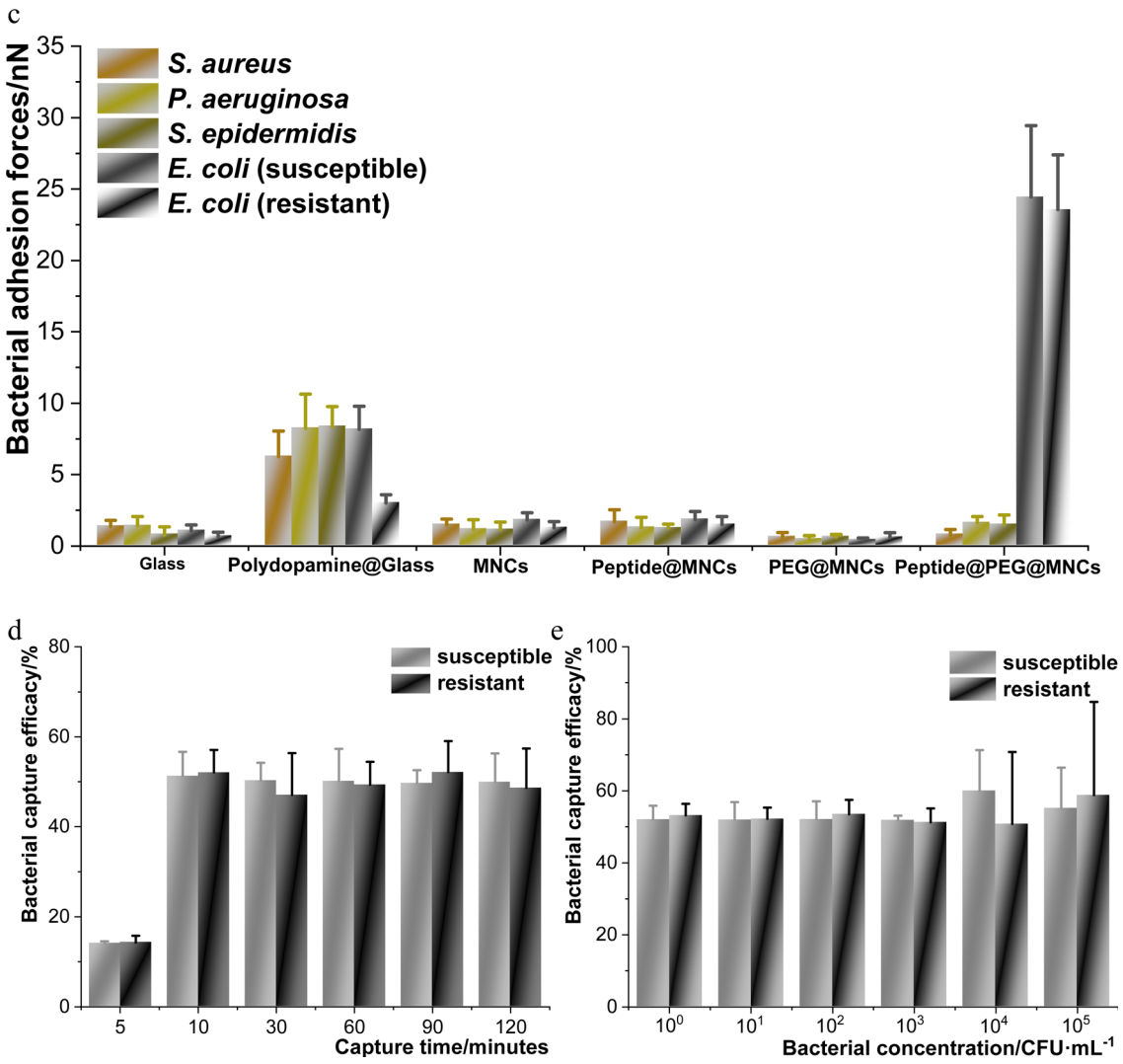

Fig. 2 *(Contd)*.

A single bacterial force microscope was utilized to better understand the interactions between the various bacterial strains and the different types of nanoclusters (Fig. 2c and Table S1†). We observed similar low adhesion forces (1.10–1.90 nN) of all assessed bacterial strains towards MNCs and peptide@MNCs. The affinity of the evaluated bacterial strains towards PEG@MNCs was even weaker, in a range of 0.40–0.62 nN, which was probably due to the well-known antifouling property of PEG.[21–24] However, the evaluated strains displayed different affinities towards peptide@PEG@MNCs. The average single bacterial adhesion forces for *S. aureus*, *P. aeruginosa*, and *S. epidermidis* were in a range of 0.77–1.60 nN, but at 24.44 and 23.56 nN for susceptible and resistant *E. coli*, respectively. The higher affinity of *E. coli* towards peptide@PEG@MNCs than other bacterial strains can explain the specific capture of *E. coli* (Fig. 2b). The capture efficacies were compromised after the rinsing process for susceptible and resistant *E. coli* at 51.3 ± 5.4% and 52.1 ± 5.0% (Fig. 2d). To the best of our knowledge, the direct measurement of specific binding of nanoclusters toward *E. coli* through FluidFM has not been reported. This study enables a quantitative biophysical investigation concerning binding specificities.

In order to investigate the impact of interaction time between *E. coli* and peptide@PEG@MNCs on the capture efficacy, the interaction was performed for 5, 10, 30, 60, 90, and 120 min (Fig. 2d). It was found that 10 minutes was sufficient for optimized interaction between *E. coli* and peptide@PEG@MNCs, and the extended interaction time up to 120 minutes did not change the capture efficacy.

The sensitivity of peptide@PEG@MNCs for *E. coli* capture with a rinsing process was further evaluated towards various bacterial concentrations (10^0–10^5 CFU mL^{-1}) (Fig. 2e). Both susceptible and resistant *E. coli* could be isolated through the specific capture by peptide@PEG@MNCs, even at a very low concentration (10^0 CFU mL^{-1}, Fig. 2e), which is 100 times lower than the reported 10^2 CFU mL^{-1}.[25] To the best of our knowledge, there is no reported system that can reach such a low concentration and, at the same time, ensure a high speci-

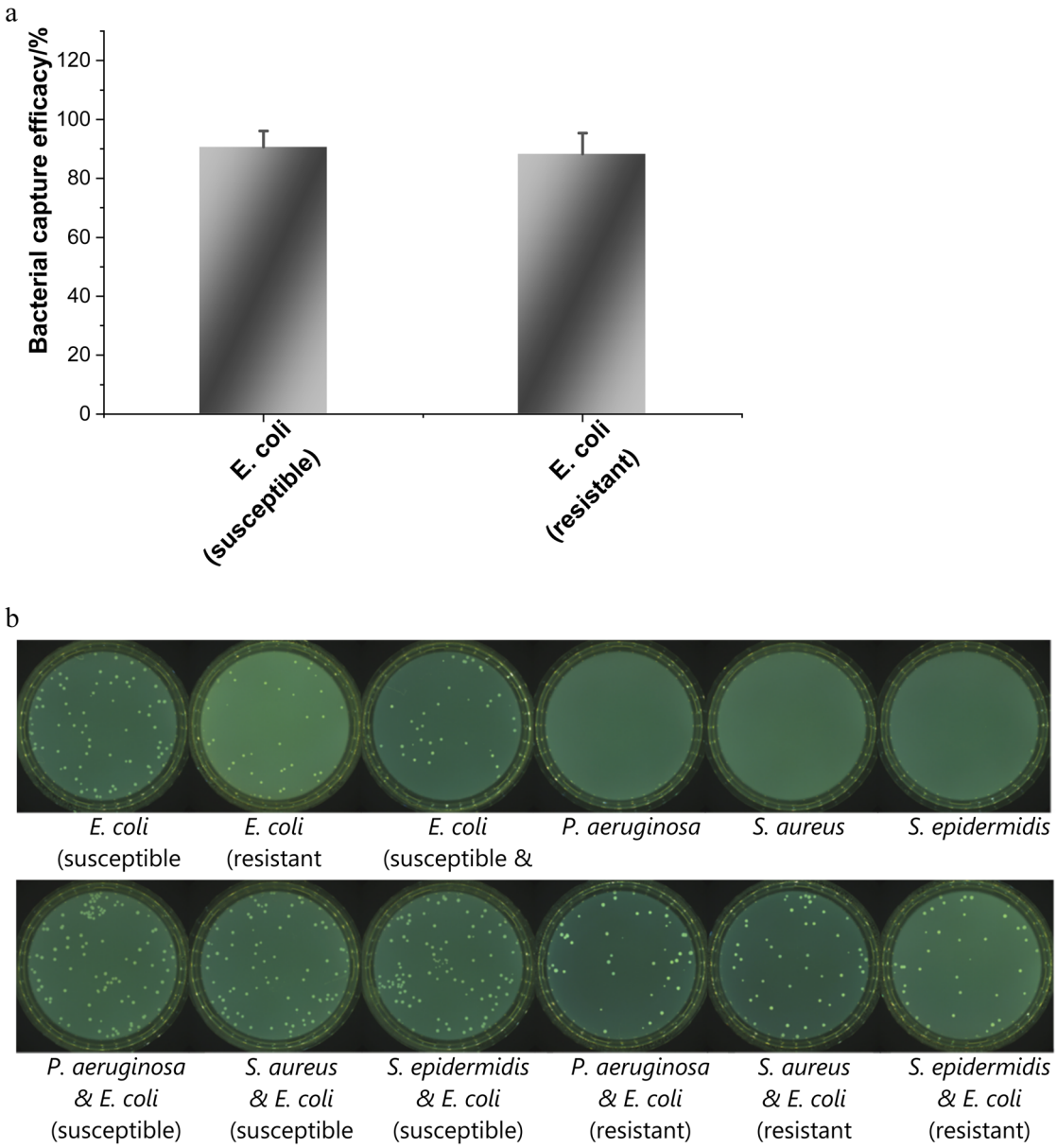

Fig. 3 Bacterial capture in artificial urine. (a) Bacterial capture efficiencies of peptide@PEG@MNCs without a rinsing process towards susceptible and resistant *E. coli*, respectively, normalized to the related initial concentration of 117 000 ± 9000 and 264 000 ± 17 000 CFU mL^{-1}. (b) Specific bacterial capture through peptide@PEG@MNCs towards susceptible *E. coli,* resistant *E. coli*, their mixture, *P. aeruginosa*, *S. aureus*, *S. epidermidis*, and susceptible or resistant *E. coli* mixed, respectively with *P. aeruginosa*, *S. aureus*, and *S. epidermidis*. (c) Specific bacterial capture efficiencies by employing peptide@PEG@MNCs towards different bacterial strains. Every capture of every single bacterial strain was normalized to the relative initial bacterial concentration (susceptible *E. coli*: 220 000 ± 20 000 CFU mL^{-1}, resistant *E. coli*: 369 000 ± 13 000 CFU mL^{-1}, *P. aeruginosa*: 754 000 ± 57 000 CFU mL^{-1}, *S. aureus*: 756 000 ± 101 000 CFU mL^{-1} and *S. epidermidis*: 7 390 000 ± 546 000 CFU mL^{-1}). The capture of bacterial mixtures was respectively normalized to susceptible *E. coli* once in the presence of susceptible *E. coli* and to resistant *E. coli* once in the presence of resistant *E. coli*. However, the mixture of susceptible and resistant *E. coli* was normalized to the sum of the initial bacterial concentration of susceptible and resistant *E. coli*. (d) The growth analysis of the specifically captured *E. coli* was performed with and without the presence of 300 μg mL^{-1} ampicillin through AquaSpark® beta-D-glucuronide. n = 3 (biological repeats), mean ± SD shown.

ficity. The specific capture towards susceptible and resistant *E. coli* was similar, probably originating from the comparable affinity of peptide@PEG@MNCs towards susceptible and resistant *E. coli* (Fig. 2c–e and Table S1†).

To evaluate the efficacy of the designed peptide@PEG@MNCs in a simulated condition, artificial urine spiked with *E. coli* was exploited to mimic the condition of wastewater collected from a urinal. The capture efficiency of *E. coli* can reach 90.6% and 88.3%, respectively, for susceptible and resistant strains without any rinsing steps (Fig. 3a). The specificity of peptide@PEG@MNCs was further investigated towards *E. coli* in artificial urine with a rinsing process. Thereby artificial

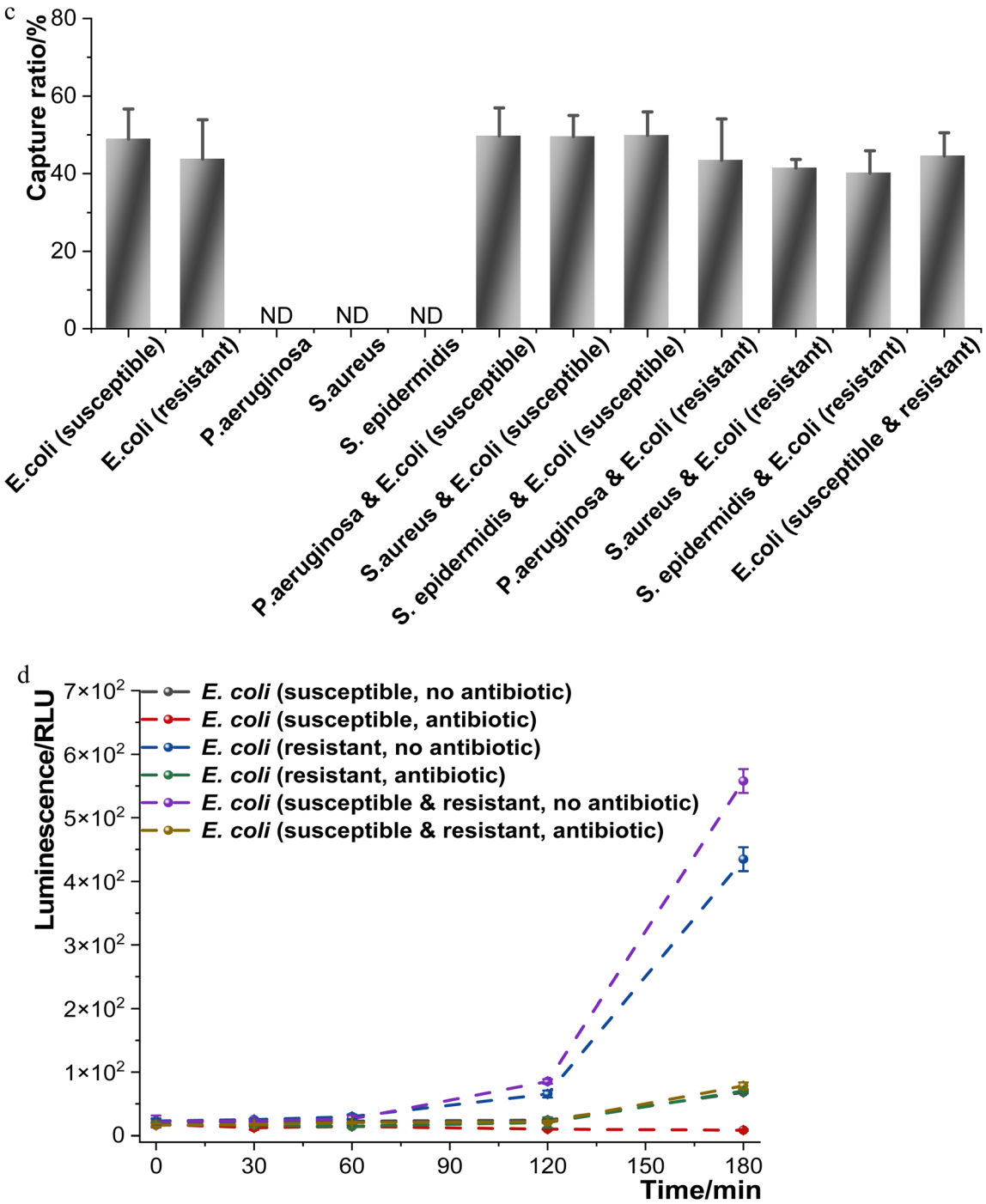

Fig. 3 *(Contd)*.

urine was spiked with *E. coli* and one of *P. aeruginosa*, *S. aureus*, and *S. epidermidis* strains. Only *E. coli* were observed on the isolated peptide@PEG@MNCs (Fig. 3b & c). The gained capture efficiency was roughly 49% and 42%, respectively, for the samples containing susceptible and resistant *E. coli*, regardless of the presence or absence of other bacteria. Thus, we could speculate that the captured bacteria from a solution of *E. coli* mixed with *P. aeruginosa, S. aureus*, or *S. epidermidis* were dominantly *E. coli*. Moreover, the results generated from PCR analysis confirmed this speculation (Fig. S3†). Hence, the designed peptide@PEG@MNCs enabled a specific capture of *E. coli* from an infected media.

The captured *E. coli* from the spiked urine were incubated with antibiotics, *e.g.*, ampicillin, and their growth was under surveillance by applying luminescent analysis (Fig. 3d) and optical density (Fig. S2a–d†). The luminescent analysis mani-

fested an intensity discrepancy after incubating for 180 minutes between collected resistant and susceptible *E. coli* (Fig. 3d). However, such a noticeable discrepancy for these samples cannot be achieved through the conventional optical density analysis (Fig. S2a–d†).

Conclusion

In this study, we successfully applied *E. coli* specific GRHIFWRRGGGHKVAPR peptide to functionalize PEGylated MNCs (peptide@PEG@MNCs), enabling isolation of various bacteria from infected media and permitting a specific capture of *E. coli* even at a concentration as low as 10^0 CFU mL^{-1}. The achieved specificity towards *E. coli* captured by peptide@PEG@MNCs was originated from the strong affinity between the assessed *E. coli* and the peptide@PEG@MNCs, directly quantitated by FluidFM. AquaSpark luminescence assay conferred a fast detection of antimicrobial resistance of the captured *E. coli*. In artificial urine, the susceptible and resistant *E. coli* can be respectively removed up to 90.6% and 88.3%, without the rinsing process, allowing the detection of antimicrobial resistance within 30 min. In addition, susceptible and resistant *E. coli* can be specifically isolated through the rinsing process and rapidly analyzed to determine antimicrobial resistance. However, the molecular biological mechanism regarding the specificity still needs to be further investigated, particularly the interaction between the peptide GRHIFWRRGGGHKVAPR and the *E. coli* membrane components. Such further investigations may explain the biomolecular interaction mechanisms of binding specificities of different biomolecules from various origins. Nevertheless, we successfully demonstrated the method developed here contributed to a fast antimicrobial resistance analysis. Our work, in terms of detection time and sensitivity, distinguishes itself from the reported methods. The peptide@PEG@MNCs manifested a diagnostic perspective in rapidly detecting resistant *E. coli* in urine to reduce drinking water contamination. The platform developed here can also be extended for other applications, such as detecting AMR *E. coli* on wound infection and catheter-associated UTIs.

Methods

Materials

Chemicals and reagents were purchased from Sigma-Aldrich (Buchs, Switzerland) in analytical purity and utilized as received unless otherwise stated. Dextran iron oxide composite nanoclusters (MNCs, product code: 09-00-132, 25 g L^{-1}, 130 nm) and PEG-NH_2 functionalized dextran iron oxide composite nanoclusters (PEGylated MNCs, product code: 09-55-132, 10 g L^{-1}, 130 nm) were exploited in aqueous suspension from micromod Partikeltechnologie GmbH (Rostock, Germany). Phosphate-buffered saline (PBS) at pH 7.4 was prepared by dissolving 8 g L^{-1} NaCl, 0.2 g L^{-1} KH_2PO_4, and 1.44 g L^{-1} Na_2PO_4 in distilled water. Bacterial growth medium (LB broth) was prepared by dissolving 10 g L^{-1} tryptone, 5 g L^{-1} yeast extract, and 5 g L^{-1} NaCl in distilled water. Broth media of an adjusted pH 7.4 was prepared by dissolving 5 g L^{-1} peptone, 5 g L^{-1} NaCl, 2 g L^{-1} yeast extract, and 1 g L^{-1} beef extract. Artificial urine was prepared[26] by dissolving 1.7 g L^{-1} Na_2SO_4, 0.25 g L^{-1} $C_5H_4N_4O_3$, 0.72 g L^{-1} $Na_3C_6H_5O_7{\cdot}2H_2O$, 0.881 g L^{-1} $C_4H_7N_3O$, 15 g L^{-1} CH_4N_2O, 2.308 g L^{-1} KCl, 1.756 g L^{-1} NaCl, 0.185 g L^{-1} $CaCl_2$, 1.266 g L^{-1} NH_4Cl, 0.035 g L^{-1} $K_2C_2O_4{\cdot}H_2O$, 1.082 g L^{-1} $MgSO_4$ $7H_2O$, 2.912 g L^{-1} NaH_2PO_4 $2H_2O$, and 0.831 g L^{-1} $Na_2HPO_4{\cdot}2H_2O$ in distilled water.

Functionalization kinetics of magnetic nanoclusters

A peptide (GRHIFWRRGGGHKVAPR, final concentration of 0.02 mM, 0.2 mM, 1 mM, 2 mM, and 20 mM) specific to *E. coli*, screened from bacteriophage display library,[19] was mixed respectively with MNCs and PEGylated MNCs of a final concentration 9 g L^{-1} for both NMCs. All mixtures were shaken for 2 hours at 100 rpm and 25 °C. Subsequently, the MNCs in each suspension were collected and rinsed by PBS three times by centrifugations at 14 400 rpm and 25 °C. After each centrifugation, the supernatant was removed and replaced by the same amount of fresh PBS.

XPS analysis

An X-ray photoelectron spectroscopy (XPS, PHI 5000 VersaProbe II instrument with a monochromatic AlKα X-ray source, USA) was applied to understand the surface chemical properties of the samples.[27–34]

Vibrating sample magnetometry

Each vacuum-dried sample was added into a polymer-sample holder and measured by applying vibrating sample magnetometry (VSM) in a physical properties measurement system (PPMS, Version P525, Quantum Design GmbH, Germany) of Quantum Design at a maximum magnetic field of 3T.[35]

Dynamic light scattering (DLS)

The hydrodynamic size of different MNCs samples was measured with a DLS instrument (ZetaSizer90, Malvern) at a refractive index of iron oxide (n = 2.918). All the measured MNCs suspensions were diluted to a final concentration of 0.9 g L^{-1} and were briefly sonicated for 30 s before each analysis.[28,35,36]

TEM analysis

TEM analysis was carried out by exploiting a JEOL TEM equipped with an in-column Omega-type energy filter (JEM-2200FS, Joel, Japan).[37–44] 5 μL of the sample suspension after a 100-fold dilution was depleted to a TEM grid (Carbon Film Supported Copper Grid, 200 Meshes, Electron Microscopy Sciences, USA) till the solvent was fully evaporated.[45–50]

Cytotoxicity analysis

Cytotoxicity analysis towards PEG@MNCs and peptide@PEG@MNCs was carried out with normal human dermal fibroblasts (nHDFs, female, Caucasian, skin/temple, PromoCell, C-12352). The sample was centrifugated, and the supernatant was replaced with DMEM (Dulbecco's Modified Eagle Medium) containing 1% penicillin/streptomycin/neomycin (PSN) to a final concentration of 9 g L^{-1} considered as no dilution. Each sample was parallelly measured with negative control (empty wells) and its sequential dilutions (2×, 4×, 8×, 16×, 32×, 64×, and 128×). 10 000 nHDFs in 100 μL DMEM containing 10% foetal calf serum (FCS) were added into every well (TPP, Trasadingen, Switzerland) and incubated for 24 hours before interacting with sample solutions. Then, the nHDFs were incubated again for 24 hours with 100 μL 95% sample solution diluted by FCS. The viability of nHDFs measured from the negative control was considered 100%, and that interacted with 1% Triton X-100 in DMEM containing 5% FCS was regarded as the positive control. The viability analysis of the nHDFs was performed with MTS [(3-(4,5-dimethylthiazol-2-yl)-5-(3-carboxymethoxyphenyl)-2-(4-sulfophenyl)-2*H*-tetrazolium)] assay through absorbance at 490 nm to evaluate metabolic activity of the nHDFs.[51–53]

Bacterial preparation

Escherichia coli DSMZ 30083, *Pseudomonas aeruginosa* DSMZ 1117, *Staphylococcus aureus* ATCC 6538, *Staphylococcus epidermidis* ATCC 49461, and *Escherichia coli* DSMZ 22312 were employed in the bacterial capture assays. One bacterial colony of each bacterial strain from an agar plate was collected and incubated in 10 mL LB in a 50 mL Falcon tube at 160 rpm and 37 °C overnight. 100 μL overnight culture was transferred into 10 mL fresh LB and then cultivated for approximately 2 h to reach exponential growth.[54]

Antimicrobial resistance (AMR) detection

Escherichia coli DSMZ 30083 and *Escherichia coli* DSMZ 22312 were incubated in 10 mL LB containing 300 μg mL^{-1} ampicillin in a 50 mL Falcon tube at 160 rpm and 37 °C overnight in order to determine bacterial sensitivity and resistance to ampicillin. The overnight bacterial culture of *Escherichia coli* DSMZ 30083 and *Escherichia coli* DSMZ 22312 in LB containing 300 μg mL^{-1} ampicillin displayed a clear and turbulent bacterial suspension, respectively. Consequently, *Escherichia coli* DSMZ 30083 and *Escherichia coli* DSMZ 22312, as revealed, are respectively susceptible and resistant to ampicillin. *Escherichia coli* DSMZ 30083 is therefore referred to as susceptible *E. coli*, and *Escherichia coli* DSMZ 22312 is analogously referred to as resistant *E. coli.* The collected bacteria, through magnetic separation, were resuspended in Broth media. AquaSpark® beta-D-glucuronide (product Code: A-8175_P00, Biosynth AG, Staad, Switzerland) was meanwhile diluted by Trisma Buffer pH 7.0 containing 1 mM $MgCl_2$ to a concentration 0.5 mM containing 1 g L^{-1} polymyxin B sulfate and 0.5 g L^{-1} lysozyme from chicken egg white. 0.180 mL bacterial suspension was subsequently incubated with 20 μL diluted AquaSpark® solution for 30 min. Then luminescence was measured by a plate reader (PowerWave HT, BioTek instruments Inc., U.S.A.). Optical density (OD_{600})[55] was always measured before adding the detection solution to the bacterial suspension through a plate reader (PowerWave HT, BioTek instruments Inc., U.S.A.).

Bacterial specific capture

The bacterial cultures of susceptible and resistant *E. coli*, *P. aeruginosa, S. aureus*, and *S. epidermidis* were diluted with PBS buffer as reported[56–58] to around 10^6 colony forming units (CFU) mL^{-1}. Then, 500 μL bacterial suspension interacted (shaking at 160 rpm) respectively with 50 μL peptide-modified PEG@MNCs, 50 μL peptide interacted MNCs, 50 μL PEG@MNCs and 50 μL MNCs for 10 min at 37 °C. Afterward, these suspensions were settled under a magnetic field for 5 min, and the clear supernatants were subsequently replaced with 550 μL fresh PBS. This rinsing process was processed 4 times more. The collected samples were further diluted with fresh PBS, and thereafter 100 μL liquid sample was plated on PC-agar plates with three replicates. Observing bacteria on PC-agar plates was carried out after incubating the PC-agar plates for 12 hours at 37 °C. This specific capture was also executed based on different times of the rinsing process: from no rinsing to 5 times rinsing.

Adhesion force analysis between bacteria and nanoclusters

MNCs (non-functionalized/functionalized on MNCs/PEG@MNCs) were immobilized onto glass-bottom microscopy dishes (GWSB-5040, WillCo-Dish, Amsterdam, Netherlands) in order to facilitate the force spectroscopy characterization. 2 mL 9 g L^{-1} MNCs were added into the microscopy dishes with polydopamine-coated glass-bottom. The method, as reported, was utilized to coat the glass-bottom microscopy dishes with polydopamine.[22,23,59] Briefly, the bottom glass of the microscopy dishes was rinsed with 2-propanol with sonication and subsequently with deionized water. Afterward, N_2-stream was exploited to dry the rinsed bottom glass of the microscopy dishes before being treated with air plasma for 120 seconds (Plasma Cleaner PD-32G, Harrick Plasma, USA). 4 mL 4 g L^{-1} polydopamine (in 10 mM TRIS HCl, pH 8.5) was used to coat the rinsed bottom glass for 60 minutes before an extensive rinsing with PBS buffer (pH 7.4). The MNCs were then added to the coated glass surfaces for the immobilization of 60 minutes. Non-immobilized MNCs were washed away with PBS buffer (pH 7.4). The microscopy dishes immobilized with MNCs were immersed with 4 mL PBS buffer (pH 7.4) for a good immersion of the FluidFM cantilever.

The Flex Bio-AFM (Nanosurf, Switzerland) and the digital pressure controller (Cytosurge, Switzerland) were similarly used as the reported method.[24] According to the reported method, single-bacteria force spectroscopy was similarly measured and analyzed at room temperature in PBS (pH 7.4) with susceptible and resistant *E. coli*, *P. aeruginosa*, *S. aureus*, and *S. epidermidis.*[24]

Bacterial specific capture rate

The specific capture rate was performed similarly to the assay of bacterial specific capture. However, the incubation time of bacterial suspension and each MNCs was defined as 5 min, 10 min, 30 min, 60 min, 90 min, and 120 min.

The sensitivity of the bacterial specific capture

The sensitivity of the specific capture was carried out similarly to the assay of bacterial specific capture. However, the initial bacterial suspensions before incubation with modified PEG@MNCs were further diluted as 10, 100, 1000, 10 000, 100 000, and 1 000 000 folds.

Bacterial specific capture in artificial urine

Bacterial specific capture in artificial urine was similarly carried out as in the assay of bacterial specific capture. Bacterial suspension mixtures were also prepared as follows with each bacteria of 10^6 CFU mL^{-1}: susceptible *E. coli* & *P. aeruginosa*, susceptible *E. coli* & *S. aureus*, susceptible *E. coli* & *S. epidermidis*, resistant *E. coli* & *P. aeruginosa*, resistant *E. coli* & *S. aureus*, resistant *E. coli* & *S. epidermidis*, and susceptible *E. coli* & resistant *E. coli*. Moreover, the resistance of the captured bacteria was analyzed through the aforementioned assay.

Polymerase chain reaction (PCR) analysis

Primers (forward primer targeting *E. coli*: 5′-CTGCTTCTTTTAAGCAACTGGCGA-3′ and reverse primer targeting *E. coli*: 5′-ACCAGACCCAGCACCAGATAAG-3′; 16SSAIII-SA:5′-TATAGATGGATCCGCGCT-3′ and 16SSAIV-SA: 5′-GATTAGGTACCGTCAAGAT-3′; FtoxA-PA: 5′-TTCGTCAGGGCGCACGAGAGCA-3′ and RtoxA-PA: 5′-TCTCCAGCGGCAGGTGGCAAG-3′) were utilized to amplify the region from the 5′ of the upstream to the 3′ of the downstream region of lacY gene of *E. coli*. Such analyses were conducted by using 200 μL captured bacteria as DNA source, 200 μM nucleotides (N0447S, NEB, USA), adequate primers (0.5 μM), 3% DMSO, 1× Buffer Phusion HF, and 1 unit per mL Phusion DNA Polymerase (Phusion High-Fidelity DNA Polymerase, M0530, NEB, USA). Cycling conditions were 98 °C for 360 s, then followed by 31 cycles of 98 °C for 10 s, 58 °C for 30 s, 72 °C for 90 s, and a final extension at 72 °C for 300 s. The generated products were separated by electrophoresis at 100 V for 60 minutes in 1% (w/v) agarose gel (V3125, Promega, Spain). The size obtained after every amplicon was analyzed in line with the 1 kb DNA ladder (GeneRuler 1 kb DNA Ladder, SM0333, Thermo Scientific, USA).

Author contributions

F. Pan and Q. Ren both conceptualized and supervised this work and conceived the experiments. Q. Ren initiated the idea of this work. F. Pan carried out the experiments. F. Pan and Q. Ren drafted this manuscript. S. Altenried contributed her microbiological knowledge and participated in the microbiology tests. S. Scheibler contributed valuable knowledge and expertise in characterizing magnetic nanoclusters. Fei Pan: conceptualization, methodology, software, validation, formal analysis, investigation, visualization, supervision, project administration, writing – original draft, writing – review & editing. Stefanie Altenried: methodology, validation, investigation. Subas Scheibler: methodology, investigation, validation. Qun Ren: conceptualization, methodology, validation, formal analysis, investigation, supervision, project administration, writing – original draft, writing – review & editing.

Data availability

The data that support the findings of this study are available from the corresponding authors upon reasonable request.

Conflicts of interest

There are no conflicts to declare.

Acknowledgments

The authors acknowledge Irene Rodriguez Fernandez for her technical input. The authors thank Dr Mario Hupfeld and Dr Lukas Tanner from NEMIS Technologies AG (Dübendorf, Switzerland), and Dr Julian Ihssen from Biosynth AG (Staad, Switzerland) for their kind support and donation of the AquaSpark® beta-D-glucuronide luminescent probe. The authors would like to thank Nico Strohmeyer and O. Guillaume-Gentil for their kind input regarding BioAFM. Schemes 1b and c were created with BioRender.com granted by a proper license.

References

1 H. Nguendo-Yongsi, Microbiological evaluation of drinking water in a sub-Saharan urban community (Yaounde), *Am. J. Biochem. Mol. Biol.*, 2011, **1**, 68–81.
2 C. Delaire, *et al.*, How much will it cost to monitor microbial drinking water quality in sub-Saharan Africa?, *Environ. Sci. Technol.*, 2017, **51**, 5869–5878.
3 W.H.O., *Drinking-water,* 2021. **https://www.who.int/news-room/fact-sheets/detail/drinking-water** (accessed on November 16th, 2021).
4 F. Pan, *Fighting Antimicrobial Resistant (AMR) Bacteria: from Bacteriophage-Based Specific Capture to Controlled Killing*, ETH Zurich, 2022.
5 E. Sanganyado and W. Gwenzi, Antibiotic resistance in drinking water systems: Occurrence, removal, and human health risks, *Sci. Total Environ.*, 2019, **669**, 785–797.
6 S. M. Vranic, N. Zatric, V. Rebic, M. Aljicevic and A. Abdulzaimovic, The most frequent isolates from outpatients with urinary tract infection, *Mater. Sociomed.*, 2017, **29**, 17–20.

7 S. C. Yang, C. H. Lin, I. A. Aljuffali and J. Y. Fang, Current pathogenic Escherichia coli foodborne outbreak cases and therapy development, *Arch. Microbiol.*, 2017, **199**, 811–825.
8 S. J. Olsen, *et al.*, A waterborne outbreak of Escherichia coli O157:H7 infections and hemolytic uremic syndrome: implications for rural water systems, *Emerging Infect. Dis.*, 2002, **8**, 370–375.
9 M. Lattuada, *et al.*, Theranostic body fluid cleansing: rationally designed magnetic particles enable capturing and detection of bacterial pathogens, *J. Mater. Chem. B*, 2016, **4**, 7080–7086.
10 J. Choi, *et al.*, A rapid antimicrobial susceptibility test based on single-cell morphological analysis, *Sci. Transl. Med.*, 2014, **6**, 267ra174.
11 J. W. Kretzer, M. Schmelcher and M. J. Loessner, Ultrasensitive and fast diagnostics of viable Listeria cells by CBD magnetic separation combined with A511: luxAB detection, *Viruses*, 2018, **10**, 626.
12 I. Choopara, *et al.*, Fluorometric paper-based, loop-mediated isothermal amplification devices for quantitative point-of-care detection of methicillin-resistant Staphylococcus aureus (MRSA), *ACS Sens.*, 2021, **6**, 742–751.
13 P. Nag, K. Sadani, S. Mukherji and S. Mukherji, Beta-lactam antibiotics induced bacteriolysis on LSPR sensors for assessment of antimicrobial resistance and quantification of antibiotics, *Sens. Actuators, B*, 2020, **311**, 127945.
14 A. Lesniewski, *et al.*, Antibody Modified Gold Nanoparticles for Fast and Selective, Colorimetric T7 Bacteriophage Detection, *Bioconjugate Chem.*, 2014, **25**, 644–648.
15 H. Z. Lai, S. G. Wang, C. Y. Wu and Y. C. Chen, Detection of Staphylococcus aureus by Functional Gold Nanoparticle-Based Affinity Surface-Assisted Laser Desorption/Ionization Mass Spectrometry, *Anal. Chem.*, 2015, **87**, 2114–2120.
16 R. A. Bohara and S. H. Pawar, Innovative Developments in Bacterial Detection with Magnetic Nanoparticles, *Appl. Biochem. Biotechnol.*, 2015, **176**, 1044–1058.
17 A. Ojha, Nanomaterials for removal of waterborne pathogens: opportunities and challenges, *Waterborne Pathog.*, 2020, 385–432.
18 S. Portsmouth, *et al.*, Cefiderocol versus imipenem-cilastatin for the treatment of complicated urinary tract infections caused by Gram-negative uropathogens: a phase 2, randomised, double-blind, non-inferiority trial, *Lancet Infect. Dis.*, 2018, **18**, 1319–1328.
19 M. Tanaka, I. H. Harlisa, Y. Takahashi, N. A. Ikhsan and M. Okochi, Screening of bacteria-binding peptides and one-pot ZnO surface modification for bacterial cell entrapment, *RSC Adv.*, 2018, **8**, 8795–8799.
20 W. Pajerski, *et al.*, Attachment efficiency of gold nanoparticles by Gram-positive and Gram-negative bacterial strains governed by surface charges, *J. Nanopart. Res.*, 2019, **21**, 186.
21 S. Lowe, N. M. O'Brien-Simpson and L. A. Connal, Antibiofouling polymer interfaces: poly(ethylene glycol) and other promising candidates, *Polym. Chem.*, 2015, **6**, 198–212.
22 F. Guo, *et al.*, Robust Antibacterial Activity of Xanthan-Gum-Stabilized and Patterned CeO_2–x–TiO2 Antifog Films, *ACS Appl. Mater. Interfaces*, 2022, **14**, 44158–44172.
23 F. Pan, *et al.*, Advanced antifouling and antibacterial hydrogels enabled by controlled thermo-responses of a biocompatible polymer composite, *Biomater. Sci.*, 2022, **10**, 6146–6159.
24 F. Pan, *et al.*, Uncoupling bacterial attachment on and detachment from polydimethylsiloxane surfaces through empirical and simulation studies, *J. Colloid Interface Sci.*, 2022, **622**, 419–430.
25 J. W. Kretzer, M. Schmelcher and M. J. Loessner, Ultrasensitive and Fast Diagnostics of Viable Listeria Cells by CBD Magnetic Separation Combined with A511::luxAB Detection, *Viruses*, 2018, **10**, 626.
26 N. Sarigul, F. Korkmaz and İ. Kurultak, A new artificial urine protocol to better imitate human urine, *Sci. Rep.*, 2019, **9**, 20159.
27 J. Wei, *et al.*, Hofmeister Effect-Inspired Ti3C2Tx MXene-Based Robust, Multifunctional Hydrogels, *Composites, Part A*, 2023, **172**, 107626.
28 F. Pan, S. Altenried, S. Scheibler, A. H. C. Anthis and Q. Ren, Specific capture of Pseudomonas aeruginosa for rapid detection of antimicrobial resistance in urinary tract infections, *Biosens. Bioelectron.*, 2023, **222**, 114962.
29 R. Zhang, *et al.*, Scalable manufacturing of light, multifunctional cellulose nanofiber aerogel sphere with tunable microstructure for microwave absorption, *Carbon*, 2023, **203**, 181–190.
30 N. Wu, *et al.*, Ultrafine Cellulose Nanocrystal-Reinforced MXene Biomimetic Composites for Multifunctional Electromagnetic Interference Shielding, *Sci. China Mater.*, 2022, **66**, 1597–1606.
31 J. Wei, *et al.*, Bioinspired cellulose-integrated MXene-based hydrogels for multifunctional sensing and electromagnetic interference shielding, *Interdiscip. Mater.*, 2022, **1**, 495–506.
32 Y.-S. Lai, *et al.*, Energy-Yielding Mini Heat Thermocells with WS2 Water-Splitting Dual System to Recycle Wasted Heat, *ACS Appl. Energy Mater.*, 2019, **2**, 7092–7103.
33 W.-F. Tong, X.-L. Liu, F. Pan, Z.-Q. Wu and W.-W. Jiang, Protein adsorption and cell adhesion on RGD-functionalized silicon substrate surfaces, *Chin. J. Polym. Sci.*, 2013, **31**, 495–502.
34 N. Wu, *et al.*, Ultrathin Cellulose Nanofiber Assisted Ambient-Pressure-Dried, Ultralight, Mechanically Robust, Multifunctional MXene Aerogels, *Adv. Mater.*, 2022, **35**, 2207969.
35 F. Pan, *et al.*, Ultrafast Determination of Antimicrobial Resistant Staphylococcus aureus Specifically Captured by Functionalized Magnetic Nanoclusters, *ACS Sens.*, 2022, **7**, 3491–3500.
36 P.-Y. Kung, S.-L. Cai, F. Pan, T.-W. Shen and Y.-H. Su, Photonic Fano Resonance of Multishaped Cu2O Nanoparticles on ZnO Nanowires Modulating Efficiency of Hydrogen Generation in Water Splitting Cell, *ACS Sustainable Chem. Eng.*, 2018, **6**, 6590–6598.

37 J. Wei, *et al.*, Bio-Inspired Additive Manufacturing of Hierarchical Materials: From Bio-Structures to Functions, *Research*, 2023, **6**, 0164.
38 Y.-K. Liao, Y.-S. Lai, F. Pan and Y.-H. Su, Hybrid-biotaxonomy-like machine learning enables an anticipated surface plasmon resonance of Au/Ag nanoparticles assembled on ZnO nanorods, *J. Mater. Chem. A*, 2023, **11**, 11187–11201.
39 B. Li, *et al.*, Graphene Oxide-Assisted Multiple Cross-Linking of MXene for Large-Area, High-Strength, Oxidation-Resistant, and Multifunctional Films, *Adv. Funct. Mater.*, 2023, **33**, 2213357.
40 W. Li, *et al.*, Au nanoparticle decorated WO3 nanorods with enhanced optical limiting activity, *Opt. Mater. Express*, 2020, **10**, 2655–2668.
41 Y. Yang, *et al.*, Biomimetic Porous MXene Sediment-Based Hydrogel for High-Performance and Multifunctional Electromagnetic Interference Shielding, *ACS Nano*, 2022, **16**, 15042–15052.
42 J. Wei, R. Wang, F. Pan and Z. Fu, Polyvinyl Alcohol/Graphene Oxide Conductive Hydrogels via the Synergy of Freezing and Salting Out for Strain Sensors, *Sensors*, 2022, **22**, 3015.
43 F. Pan, H.-L. Chen, Y.-H. Su, Y.-H. Su and W.-S. Hwang, Inclusions properties at 1673 K and room temperature with Ce addition in SS400 steel, *Sci. Rep.*, 2017, **7**, 2564.
44 F. Pan, Y.-H. Su, J. Augusto, W.-S. Hwang and H.-L. Chen, Optical inclusion transformation with different amount of cerium addition during solidification of SS400 steel, *Opt. Quantum Electron.*, 2016, **48**, 536.
45 F. Pan, C.-C. Wu, Y.-L. Chen, P.-Y. Kung and Y.-H. Su, Machine learning ensures rapid and precise selection of gold sea-urchin-like nanoparticles for desired light-to-plasmon resonance, *Nanoscale*, 2022, **14**, 13532–13541.
46 R. Yu, *et al.*, Quantitative Determination of Airborne Redox-Active Compounds Based on Heating-Induced Reduction of Gold Nanoparticles, *Anal. Chem.*, 2021, **93**, 14859–14868.
47 P.-Y. Kung, F. Pan and Y.-H. Su, Spintronic hydrogen evolution induced by surface plasmon of silver nanoparticles loaded on Fe- and Co-doped ZnO nanorods, *J. Mater. Chem. A*, 2021, **9**, 24863–24873.
48 C.-C. Wu, F. Pan and Y.-H. Su, Surface Plasmon Resonance of Gold Nano-Sea-Urchins Controlled by Machine-Learning-Based Regulation in Seed-Mediated Growth, *Adv. Photonics Res.*, 2021, **2**, 2100052.
49 P.-Y. Kung, F. Pan and Y.-H. Su, Gold Nanoparticles on TM: ZnO (TM: Fe, Co) as Spinplasmon-Assisted Electro-Optic Reaction Modulator in Solar-to-Hydrogen Water Splitting Cell, *ACS Sustainable Chem. Eng.*, 2020, **8**, 14743–14751.
50 M.-Y. Tseng, Y.-H. Su, Y.-S. Lai, F. Pan and P.-Y. Kung, Cobalt–Citrate Metal–Organic-Framework UTSA-16 on TiO2 Nanoparticles, *IOP Conf. Ser.: Mater. Sci. Eng.*, 2020, **720**, 012008.
51 G. Jin, *et al.*, Tissue engineered plant extracts as nanofibrous wound dressing, *Biomaterials*, 2013, **34**, 724–734.
52 P. Solar, *et al.*, Multifunctional polymeric nanoparticles doubly loaded with SPION and ceftiofur retain their physical and biological properties, *J. Nanobiotechnol.*, 2015, **13**, 14.
53 F. Pan, *et al.*, pH-responsive silica nanoparticles for triggered treatment of skin wound infections, *Acta Biomater.*, 2022, **145**, 172–184.
54 D. Hegemann, *et al.*, Plasma-deposited AgOx-doped TiOx coatings enable rapid antibacterial activity based on ROS generation, *Plasma Processes Polym.*, 2022, **19**, e2100246.
55 Y.-S. Lai, F. Pan and Y. H. Su, Firefly-like Water Splitting Cells Based on FRET Phenomena with Ultrahigh Performance over 12%, *ACS Appl. Mater. Interfaces*, 2018, **10**, 5007–5013.
56 F. Pan, *et al.*, Photo-activated titanium surface confers time dependent bactericidal activity towards Gram positive and negative bacteria, *Colloids Surf., B*, 2021, **206**, 111940.
57 F. Pan, *et al.*, Bioresponsive hybrid nanofibers enable controlled drug delivery through glass transition switching at physiological temperature, *ACS Appl. Bio Mater.*, 2021, **4**, 4271–4279.
58 F. Pan, *et al.*, A nanolayer coating on polydimethylsiloxane surfaces enables a mechanistic study of bacterial adhesion influenced by material surface physicochemistry, *Mater. Horiz.*, 2020, **7**, 93–103.
59 M. Mittelviefhaus, D. B. Müller, T. Zambelli and J. A. Vorholt, A modular atomic force microscopy approach reveals a large range of hydrophobic adhesion forces among bacterial members of the leaf microbiota, *ISME J.*, 2019, **13**, 1878–1882.